Synchronous phase-demodulation and harmonic rejection of 9-step pixelated dynamic interferograms

J. M. Padilla, M. Servin,* and J. C. Estrada

Centro de Investigaciones en Optica A. C. Loma del Bosque 115, Lomas del Campestre, C.P. 37150, Leon, Guanajuato, Mexico

mservin@cio.mx

Abstract: We propose a novel synchronous phase-demodulation of pixelated interferograms using squared 3x3 phase-shifted unit-cells. This 3x3 unit-cell is tiled over the CCD image sensor to create a two-dimensional (2D) pixelated carrier. Our synchronous phase-demodulation uses this 2D carrier to demodulate the pixelated interferogram as in the standard 2x2 unit-cell case. The main motivation behind the use of a 3x3 pixelated carrier (instead of the usual 2x2) is its higher harmonic robustness, allowing one to demodulate intensity-distorted fringe patterns. The harmonic rejection robustness of our spatial 3x3 configuration equals the robustness of the temporal least-squares 9-step phase-shifting algorithm (PSA). In other words, extending from the usual 2x2 phase-shifting unit-cell to 3x3 unit-cells, one extends the harmonic rejection of the demodulation algorithm. Finally we also prove that our proposed 9-step, 3x3 pixelated carrier uses the 2D available spectral space more efficiently than using these 9-steps in a linear spatial-carrier configuration.

OCIS codes: (120.3180) Interferometry; (120.2650) Fringe analysis.

References and Links

1. H. Schreiber and J. H. Bruning, "Phase shifting interferometry," in *Optical Shop Testing*, D. Malacara, ed. (Wiley, NJ, 2007), Chap. 14, doi: 10.1002/9780470135976.ch14
2. M. Servin, J. C. Estrada, and J. A. Quiroga, "The general theory of phase shifting algorithms," Opt. Express **17**(24), 21867–21881 (2009).
3. Y. Awatsuji, M. Sasada, and T. Kubota, "Parallel quasi-phase-shifting digital holography," Appl. Phys. Lett. **85**(6), 1069–1071 (2004).
4. J. Millerd, N. Brock, J. Hayes, M. North-Morris, M. Novak, and J. C. Wyant, "Pixelated phase-mask dynamic interferometer," Proc. SPIE **5531**, 304–314 (2004).
5. B. T. Kimbrough, "Pixelated mask spatial carrier phase shifting interferometry algorithms and associated errors," Appl. Opt. **45**(19), 4554–4562 (2006).
6. G. Rodriguez-Zurita, N. I. Toto-Arellano, C. Meneses-Fabian, and J. F. Vázquez-Castillo, "One-shot phase-shifting interferometry: five, seven, and nine interferograms," Opt. Lett. **33**(23), 2788–2790 (2008).
7. B. Kimbrough and J. Millerd, "The spatial frequency response and resolution limitations of pixelated mask spatial carrier based phase shifting interferometry," Proc. SPIE **7790**, 77900K, 77900K-12 (2010).
8. M. Servin and J. C. Estrada, "Error-free demodulation of pixelated carrier frequency interferograms," Opt. Express **18**(17), 18492–18497 (2010).
9. J. M. Padilla, M. Servin, and J. C. Estrada, "Harmonics rejection in pixelated interferograms using spatio-temporal demodulation," Opt. Express **19**(20), 19508–19513 (2011).
10. Y. Surrel, "Design of algorithms for phase measurements by the use of phase stepping," Appl. Opt. **35**(1), 51–60 (1996).
11. M. Takeda, H. Ina, and S. Kobayashi, "Fourier-transform method of fringe-pattern analysis for computer-based topography and interferometry," J. Opt. Soc. Am. A **72**(1), 156–160 (1982).
12. J. C. Estrada, M. Servin, and J. A. Quiroga, "Noise robust linear dynamic system for phase unwrapping and smoothing," Opt. Express **19**(6), 5126–5133 (2011).

#162547 - $15.00 USD Received 6 Feb 2012; revised 23 Apr 2012; accepted 30 Apr 2012; published 9 May 2012

1. Introduction

One of the most used techniques to demodulate fringe patterns in optical metrology is phase-shifting interferometry (PSI), either in the spatial or temporal domain. Temporal PSI requires a movable piston or wavelength shifting in the interferometer to introduce a piston phase-step between successive samples obtaining several phase shifted interferograms to demodulate.

In standard phase-shifting algorithms (PSAs) one usually models the fringe patterns as undistorted sinusoidal signals phase-modulated by the measuring physical variable [1,2]. But in practice, non-sinusoidal fringes are frequently obtained due to saturation of the CCD photodetector, and/or multiple beams interferences, etc [1]. These experimental errors lead to generation of harmonics of the fundamental signal (distorted fringes) which degrades the quality of the estimated phase. For a given number of phase steps, the least-squares PSAs have the highest harmonic rejection number [1]. Taking several temporal phase-shifted interferograms requires stability and fast interferometer response, which may limit its usefulness for fast measuring events. To cope with this, several authors have described spatial PSI techniques for the simultaneous acquisition of phase-shifted interferograms to lessen the stability restriction to study fast dynamic events (see for instance [3,4] and its references). The technique proposed by Millerd et al. [4] allows simultaneous encoding of 4 phase-steps in a single-image interferogram using a pixelated phase-mask (PPM) physically attached to the CCD light-sensor. The physical principle of this technique is reviewed in [4].

The PPM proposed by Millerd et al. [4] introduces 4 spatial phase-steps: $\{0,\pi/2,\pi,3\pi/2\}$ arranged in a 2x2 unit-cell. In the past, phase demodulation was locally estimated for each 2x2 unit-cell using the 4-step least-squares PSA [4]. However, in this approach the estimated signal presents significant detuning errors for a fast phase changes inside this 2x2 unit-cell [5]. To compensate for this error, some authors have proposed alternative configurations and the application of averaging algorithms [5,6], or a higher low-pass 3x3 kernel [7]. Nevertheless, this detuning error can be avoided by applying a holographic synchronous method for 2D pixelated carriers [7,8]. Recently, in [9] we have shown that synchronous, single-image demodulation of 2x2 pixelated-carrier interferograms do not to reject the complex harmonics $\{-3^{rd},+5^{th},-7^{th},+9^{th},-11^{th},...\}$. This is the same harmonics rejection robustness observed with the temporal 4-step least-squares PSA [9,10].

An educated guess to improve the harmonics rejection of 2x2 unit-cell pixelated carrier interferograms is to increase the size (phase-steps) of this unit-cell. Considering this, we propose a new 2D pixelated carrier containing 9 phase-steps within a 3x3 unit-cell. This 3x3 unit-cell is tiled to cover the whole CCD camera sensor similarly to the 2x2 unit-cell did. In the following sections we analyze our synchronous method to phase-demodulate 3x3 unit-cell pixelated interferograms. Furthermore the harmonics rejection robustness of our proposed 3x3 unit-cell (9-steps) pixelated carrier is analyzed and it is shown to be superior to the 2x2 unit-cell pixelated carrier and the linear 9-step spatial carrier modulation.

2. Synchronous phase-demodulation of pixelated phase-mask interferograms

In this section we review the synchronous demodulation method for 2D pixelated carriers and present numerical simulations to illustrate the spectral behavior of our proposal [7–9].

A useful mathematical model for an ideal pixelated phase-mask interferogram is:

$$I(x,y) = a(x,y) + b(x,y)\cos[\varphi(x,y) + \mathrm{pm}(x,y)], \qquad (1)$$

where $a(x,y)$, $b(x,y)$, $\varphi(x,y)$ are respectively the background, the local contrast and the searched phase. The pixelated carrier $\mathrm{pm}(x,y)$ represents the spatial phase-steps introduced. So both $I(x,y)$ and $\mathrm{pm}(x,y)$, are the only known terms in Eq. (1).

#162547 - $15.00 USD Received 6 Feb 2012; revised 23 Apr 2012; accepted 30 Apr 2012; published 9 May 2012

We propose a new pixelated carrier $\mathrm{pm}(x, y)$ with 9 phase-steps of $\omega_0 = 2\pi/9$ radians distributed within 3x3 unit-cells following the spiral configuration shown in Fig. 1. Mathematically one may express this 2D phase-mask as,

$$\exp[i\,\mathrm{pm}(x, y)] = \left[\sum_n \sum_m \delta(x-3m, y-3n)\right] ** \exp\left\{\frac{i\,2\pi}{9}\begin{bmatrix} 1 & 2 & 3 \\ 8 & 9 & 4 \\ 7 & 6 & 5 \end{bmatrix}\right\}, \qquad (2)$$

where $**$ represents the 2D convolution product. Note that other spatial configurations are possible, for instance a stacked configuration (not analyzed herein), which may be analyzed in a similar way.

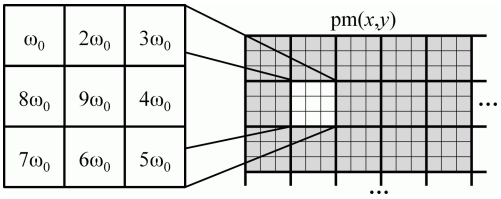

Fig. 1. Periodic distribution for our 9-steps (3x3 unit-cell) pixelated carrier phase-shifts with spiral configuration.

In synchronous spatial-carrier interferometry, the frequency of the carrier must be higher than the highest frequency component of the signal of interest, so they can be isolated by linear filtering [11]. For 2D pixelated carriers this condition may be formally stated as

$$\left|\nabla\,\mathrm{pm}(x, y)\right| > \max\left|\nabla\varphi(x, y)\right|, \qquad (3)$$

where ∇ is the gradient operator.

The first step to synchronous demodulation of pixelated phase-mask interferograms is to multiply Eq. (1) by the complex carrier in Eq. (2) [7,8].

$$\begin{aligned} I(x, y)\exp[-i\,\mathrm{pm}(x, y)] &= [a + b\cos(\varphi + \mathrm{pm})]\exp(-i\,\mathrm{pm}), \\ &= a\exp(-i\,\mathrm{pm}) + (b/2)\left\{\exp(i\varphi) + \exp[-i\,(\varphi + 2\,\mathrm{pm})]\right\}. \end{aligned} \qquad (4)$$

Applying a low-pass filter $LP[\cdot]$ to Eq. (4), preferably in the Fourier domain, the high frequency terms are rejected [7,8] (henceforth $\hat{\varphi}(x, y)$ is the estimated value) obtaining:

$$(1/2)b(x, y)\exp[i\,\hat{\varphi}(x, y)] = LP\left[\exp(-i\,\mathrm{pm})I(x, y)\right]. \qquad (5)$$

Solving Eq. (5) for the estimated phase $\hat{\varphi}(x, y)$ one obtains:

$$\tan[\hat{\varphi}(x, y)] = \frac{\mathrm{Im}\left\{LP\left[\exp(-i\,\mathrm{pm})I(x, y)\right]\right\}}{\mathrm{Re}\left\{LP\left[\exp(-i\,\mathrm{pm})I(x, y)\right]\right\}}, \qquad (6)$$

where the operators $\mathrm{Im}\{\cdot\}$ and $\mathrm{Re}\{\cdot\}$ take the imaginary and real parts of their argument. The final step is to apply a phase unwrapping process (see for instance [12]).

In Fig. 2 we present a numerical simulation for an ideal (distortion-free) sinusoidal fringe pattern phase-modulated by our proposed 3x3 (9-steps) pixelated carrier. Panel 2(a) shows the fringes produced by $\varphi(x, y)$ and its spectrum in panel 2(b). Panel 2(c) shows the pixelated interferogram produced by $\varphi(x, y) + \mathrm{pm}(x, y)$ and its spectrum in panel 2(d). Panel 2(e) shows the real part of the synchronous product (Eq. (4)) and its spectrum in panel 2(f).

#162547 - $15.00 USD Received 6 Feb 2012; revised 23 Apr 2012; accepted 30 Apr 2012; published 9 May 2012

Finally, panel 2(g) shows the demodulated phase $\hat{\varphi}(x, y)$ in Eq. (6) and the spectrum of the searched analytical signal (Eq. (5)) in panel 2(h).

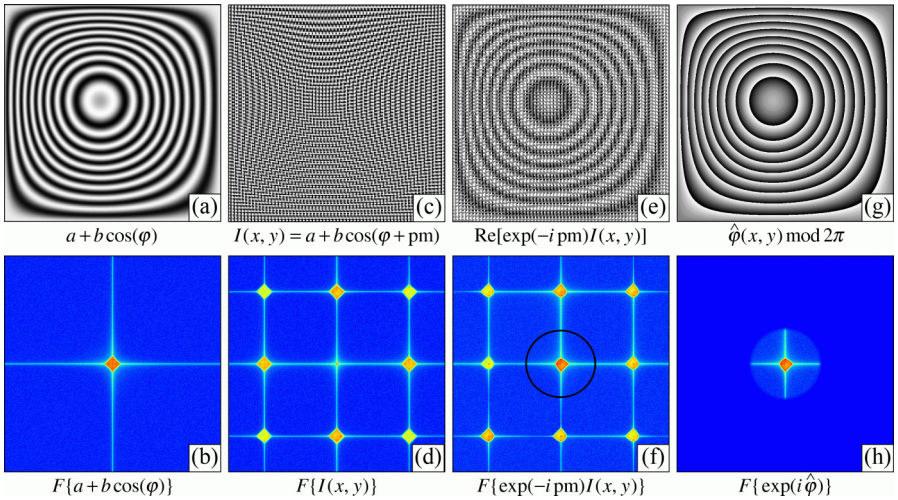

Fig. 2. The panels on this figure show our 3x3 synchronous demodulation herein proposed applied to harmonic-free interferograms. Detailed panel description is presented in the text.

By examining $F\{\exp(-i\,\mathrm{pm})I(x, y)\}$ in panel 2(f), one can see that the complex conjugate signal $\exp[-i\,\hat{\varphi}(x, y)]$ is split into 8-components separated at least by $2\pi/3$ radians from the centered searched analytical signal $\exp[i\,\hat{\varphi}(x, y)]$. Formally, the spatial frequency of the measuring phase is then restricted to:

$$\max\left|\nabla\varphi(x, y)\right| < 2\pi/6. \tag{7}$$

This is the radius of the low-pass filter (dark ring) shown in Fig. 2(f).

3. Synchronous-Fourier demodulation of intensity-distorted pixelated interferograms

Quite frequently, experimental data have systematic errors (nonlinear photodetector response, gain saturation, multiple beams interferences, etc.) which adds harmonics to the signal [1,2]. Hence an intensity-distorted fringe interferogram is obtained. One may represent this distorted (non-sinusoidal) pixelated fringe pattern by the following Fourier series,

$$I(x, y) = a(x, y) + \sum_{n=1}^{\infty} b_n(x, y)\cos\left\{n[\varphi(x, y) + \mathrm{pm}(x, y)]\right\}, \tag{8}$$

where $b_n(x, y)$ are the contrast function for the n-th harmonic; all others terms remain as previously defined. Following our synchronous 3x3 demodulation method, one forms the product $\exp[-i\,\mathrm{pm}(x, y)]I(x, y)$,

$$\exp(-i\,\mathrm{pm})I(x, y) = a\exp(-i\,\mathrm{pm}) + \sum_{n=1}^{\infty}(b_n/2)\left\{\exp[i(n-1)\,\mathrm{pm}]\exp[i(n\varphi)]\right.$$
$$\left.+\exp[-i(n+1)\,\mathrm{pm}]\exp[i(n\varphi)]\right\}. \tag{9}$$

The 2D harmonic carriers $\exp[\pm i(n\mp 1)\,\mathrm{pm}(x, y)]$ displace the analytical harmonic signals $\exp[\pm i\,n\,\varphi(x, y)]$ from the spectral origin [9]. Note that the following harmonics (taken from Eq. (9)) overlap with the desired (base-band) analytical signal $\exp[i\,\varphi(x, y)]$:

#162547 - $15.00 USD Received 6 Feb 2012; revised 23 Apr 2012; accepted 30 Apr 2012; published 9 May 2012

$$\exp[+i(n-1)\,\mathrm{pm}(x,y)] = 1, \quad \forall(x,y) \quad \text{if} \quad n = 1,10,19,28,...$$
$$\exp[-i(n+1)\,\mathrm{pm}(x,y)] = 1, \quad \forall(x,y) \quad \text{if} \quad n = 8,17,26,35,... \qquad (10)$$

The low-pass filtering (Eq. (5)) rejects the remaining harmonics (not present in Eq. (10)), so the estimated harmonic-distorted base-band analytical signal results on:

$$A\exp[i\,\hat{\varphi}(x,y)] = \{b_1\exp(i\varphi) + b_8\exp(-i8\varphi) + b_{10}\exp(i10\varphi) + b_{17}\exp(-i17\varphi) + ...\}, \quad (11)$$

where A is a proportionality constant. Usually, the energy contribution in Eq. (11) of the n-th harmonic decreases very fast $(b_n << b_1)$. For this reason, the distortion in our estimated phase $\hat{\varphi}(x,y)$ due to these harmonics, starting with the 8th harmonic in Eq. (11) is quite small.

As expected, Eq. (11) shows that our 3x3 (9-steps) pixelated carrier rejects the same harmonics as a temporal 9-steps least-squares PSA [1,2,10]. We illustrate this in Fig. 3 where the frequency transfer function (FTF) for the 9-step least-squares PSA is shown [2].

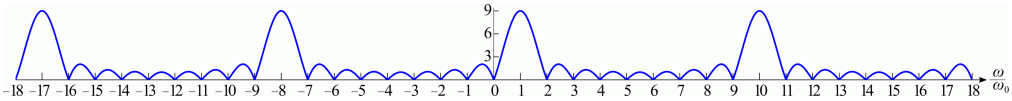

Fig. 3. Magnitude of the FTF for the temporal 9-step least-squares PSA.

Figure 4 shows a numerical simulation for a intensity-distorted (non-sinusoidal) fringe pattern phase-modulated with our 3x3 (9-steps) pixelated carrier (Eq. (2)). Panel 4(a) shows a distorted fringes interferogram and its spectrum in panel 4(b). Panel 4(c) shows the pixelated interferogram produced by $\varphi(x,y) + \mathrm{pm}(x,y)$ and its spectrum in Panel 4(d). Panel 4(e) shows the real part of the synchronous product (Eq. (9)) and its spectrum in Panel 4(f). Finally, Panel 4(g) shows the almost distortion-free demodulated phase $\hat{\varphi}(x,y)$ and the spectrum of the searched analytical signal (Eq. (11)) in panel 4(h).

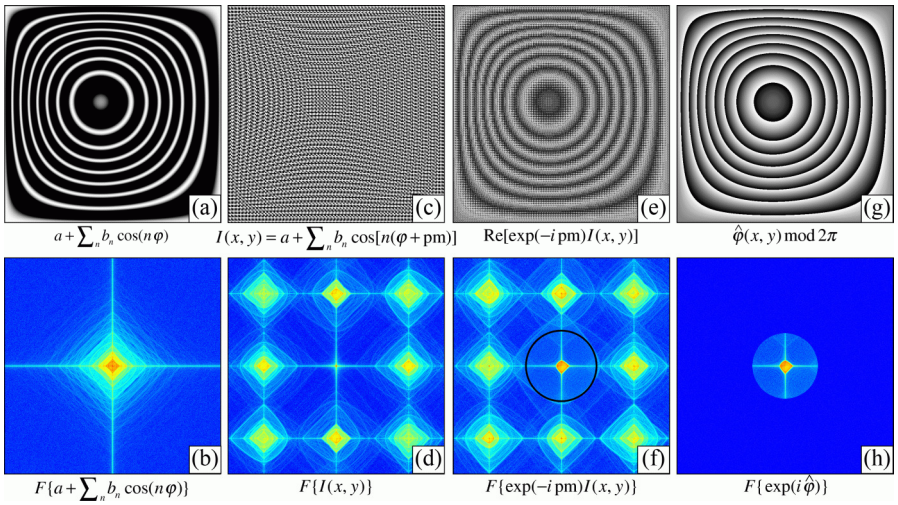

Fig. 4. The panels on this figure show the synchronous demodulating process herein proposed applied to intensity-distorted interferograms. Detailed panel description is presented in the text.

4. Harmonic rejection of the 2x2, the 3x3, and the linear 9-step pixelated carriers

Here we compare the spectral distribution, and phase-demodulation performance obtained with spatial pixelated: 2x2 circular, our 3x3 spiral, and the linear 9-step carriers (see Fig. 5). For comparative purposes, in the three cases we have applied the same low-pass filter (the small dark-ring shown in Fig. 5).

#162547 - $15.00 USD Received 6 Feb 2012; revised 23 Apr 2012; accepted 30 Apr 2012; published 9 May 2012

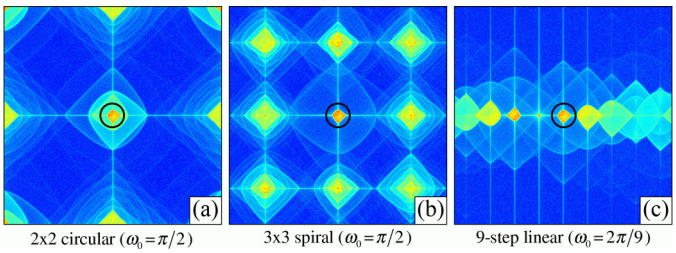

Fig. 5. Spectral distribution of distorted, non-sinusoidal interferograms using: the 2x2, the 3x3, and the linear 9-step pixelated modulating spatial carriers.

Panel 5(a) shows that the highest spectral separation (π radians) is obtained using 2x2 unit-cells, but the harmonics $\{-3^{rd},+5^{th},-7^{th},+9^{th},-11^{th},...\}$. remain at the base-band [9]. In contrast, our 3x3 pixelated keeps just the $\{-8^{th},+10^{th},-17^{th},+19^{th},...\}$ harmonics at the base-band, with spectral separation of $2\pi/3$ radians (panel 5(b)). Finally, in panel 5(c) a 9-step linear carrier spectrum is shown; the base-band region is now far more crowded with overlapping distorting harmonic energy.

Figure 6 shows the central slice of the estimated phases due to intensity-distorted fringes.

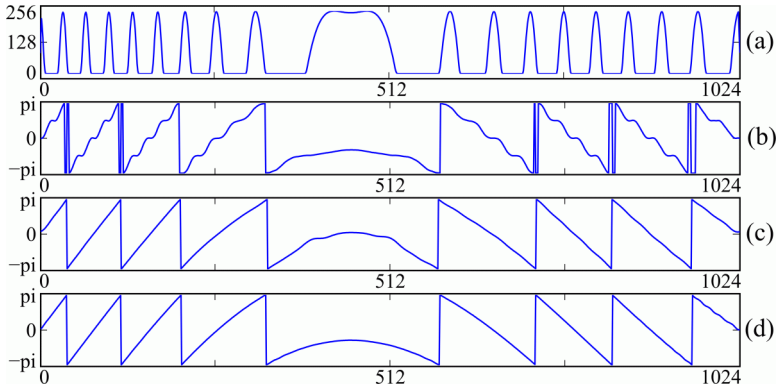

Fig. 6. Panel (a) shows the central slice of the non-sinusoidal fringe pattern. The central slices of the estimated phase using: (b) 2x2 pixelated carrier, (c) 9-step linear carrier, and (d) 3x3 pixelated carrier interferograms.

Panel 6(a) shows the amount of intensity-distortion in the fringes. Panel 6(b) shows the estimated signal $\hat{\varphi}(x,y)$ with severe harmonic distortion using a 2x2 unit-cell carrier. Figure 6(c) shows $\hat{\varphi}(x,y)$ for the 9-step linear carrier being distorted by those harmonics that overlap our searched signal at the base-band (panel 5(c)). Finally Fig. 6(d) shows the almost harmonic-free estimated phase $\hat{\varphi}(x,y)$ using our 3x3 spiral pixelated carrier demodulation.

5. Conclusion

We presented a new 3x3 unit-cell (9-steps) pixelated phase-shifting interferometry. We show that our proposed 3x3 pixelated carrier has the same harmonic rejection capability as the temporal 9-step PSA. This harmonic robustness is higher than the standard 2x2 unit-cell pixelated carrier. Also we have shown that the spectral separation of our 3x3 carrier ($2\pi/3$ radians) is higher than the 9-step spatial-carrier separation ($2\pi/9$ radians).

Acknowledgment

The authors wish to thanks the Mexican National Council for Science and Technology (CONACyT) for the financial support.

#162547 - $15.00 USD Received 6 Feb 2012; revised 23 Apr 2012; accepted 30 Apr 2012; published 9 May 2012